San Jose State University Interlibrary Services

ILLiad TN: 415418

Borrower: MFL
Borrower's TN: 9646.0

Lending String: *CSJ,CSF,CDS,UAF,CHU

Patron: Chaffey, Mark

Journal Title: Journal of engineering mechanics /

Volume: 116 **Issue:**
Month/Year: 1990
Pages: 2083-2099

Article Author:

Article Title: Raoof, M.; Axial fatigue of multi-layered strands

Imprint: New York, N.Y. ; American Society of Civ

ILL Number: 71997588

12/10/2010 05:04:50 PM

Borrowing Notes; Please don`t send directly to patron/ MLML is a part of the California State University System.

Maxcost: $20IFM

Charge:
- [ ] **IFM**
- [ ] **Invoice to follow at month's end**

Shipping Address:
CSU Moss Landing Marine Labs
Library, ILL
PO Box 450
Moss Landing, CA 95039 (TRICOR)

Fax: (831) 632-4403
Ariel:
Odyssey: mlml.calstate.illiad.oclc.org

PROBLEM REPORT

If you have experienced a problem with the delivery of the requested item, please contact us with the following information. Send back this form via fax or Ariel.

San Jose State University
Interlibrary Services
129 S. 10th St.
San Jose, CA 95192-0028

FAX: (408) 808-2077
ARIEL: 130.65.109.147

______ Pages were missing pp. ____________ to ____________

______ Edges were cut off pp. ____________ to ____________

______ Illegible copy – please resend entire item

______ Incorrect article sent

______ Not received

______ Other (please explain)

AXIAL FATIGUE OF MULTILAYERED STRANDS

By Mohammed Raoof[1]

ABSTRACT: Previously reported orthotropic sheet theory is used for obtaining estimates of interwire/interlayer contact stresses throughout realistic pretensioned multilayered structural strands. These data are used in conjunction with axial fatigue data on single wires to develop a theoretical model that predicts axial fatigue life of strands (under constant amplitude cyclic loading) from first principles. The theoretical interlayer slippage over the individual points of contact between cross-laid layers is addressed, which takes interwire friction into account. The match between the theoretical predictions and experimental fatigue data is very encouraging. Numerical examples suggest that cable axial fatigue life depends on the type of strand construction. The level of mean axial load appears to have a modest effect on the cable stress range versus fatigue life (S-N) curves. For a given wire material, the endurance limit is found to increase with increasing level of mean axial load, becoming practically constant for mean axial loads greater than 40% of the cable maximum breaking load. Different types of cable construction are found to possess significantly different levels of endurance limit.

INTRODUCTION

The safety of the many deep-water platform concepts is, among other considerations, strongly dependent on the reliability of the anchoring systems, which should have a high level of integrity and whose costs of installation and replacement are very high. Since the mid-1970s there has been a significant increase in the sizes of steel strand being considered by the offshore oil industry: 127-mm-diameter spiral strands were used for the catenary moorings of the (Exxon) Lena Guyed Tower and 137-mm-diameter strands were employed on the (Woodside) North Rankin A platform.

Many of the factors affecting the service life of large-diameter cables could be studied much more economically and quickly by using smaller-scale model strands (or wires), provided only that the results so obtained could be extrapolated to those for the prototype size with sufficient confidence. To do this, a sound understanding of the fundamental factors influencing cable fatigue performance is necessary. The work reported here may be regarded as a step towards this goal. The interested reader may also refer to the work of Chien et al. (1988), who employed dimensional analysis with similar objectives in mind.

In a series of recent publications (Hobbs and Raoof 1982; Raoof and Hobbs 1988a), an analytical model backed by large-scale experimental results has been developed, which, unlike previously published theories, takes interwire/interlayer contact forces and their associated relative displacements into account. In what follows, the model will be extended to predict axial fatigue life of strands away from end terminations using fatigue data on single component wires.

On the analytical side, Leissa (1959), Starkey and Cress (1959), Bert and

[1]Sr. Lect., Civ. and Struct. Engrg. Dept., South Bank Polytech., Wandsworth Rd., London SW8 2JZ, U.K.

Note. Discussion open until March 1, 1991. To extend the closing date one month, a written request must be filed with the ASCE Manager of Journals. The manuscript for this paper was submitted for review and possible publication on August 17, 1989. This paper is part of the *Journal of Engineering Mechanics*, Vol. 116, No. 10, October, 1990. ©ASCE, ISSN 0733-9399/90/0010-2083/$1.00 + $.15 per page. Paper No. 25105.

Stein (1962), and Phillips et al. (1980) have attempted theoretical studies of interwire contact stresses. All of these theoretical works ignored interwire frictional effects and no attempt was made to correlate the so-obtained values of interwire contact stresses with experimental data. Recently, Knapp and Chiu (1988), who addressed the axial fatigue problem of electromechanical strands, developed a promising theoretical model backed by fatigue experimental data. Their model ignored interwire/interlayer friction and displacement and was developed for an electromechanical strand with two layers of helical wires. None of these references takes into account the distribution of interlayer clench forces into hoop and radial components in the multilayered strands. For a recent general review of the state of wire-rope research, the interested reader may refer to the survey by Chaplin and Potts (1988).

In this paper, the previously reported orthotropic sheet theory will be used to obtain estimates of interwire/interlayer contact forces and their associated relative displacements in multilayered helical strands. Using such data, the interwire maximum Hertzian stress will be calculated, which, in conjunction with fatigue data on single wires, provides estimates of cable fatigue life under cyclic axial loading. The theory also casts some light on the relevance of cross-wire (trellis) interlayer movements (and hence fretting) to strand axial fatigue life prediction. Such interwire movements have been found (Raoof 1990b) to be the principal cause of individual wire failures in the case of the free-bending fatigue performance of helical strands in the vicinity of end terminations with some degree of fixity.

Orthotropic Sheet Theory

Background

Full details of the theory have been given elsewhere (Hobbs and Raoof 1982; Raoof and Hobbs 1988a) and will not be repeated here due to space limitations. Only a few of its salient features that are of direct relevance to the present paper will be briefly discussed, and a summary of some of its directly relevant final formulations will be presented for completeness.

In essence, the individual layers of wires in a multilayered strand are treated as a series of partly self-prestressed cylindrical orthotropic sheets whose nonlinear elastic properties are averaged to form an equivalent continuum. The analysis is developed for a strand with its ends fixed against rotation, and is based on the main assumption that with zero axial load on the cable the wires in each layer are just touching each other. Therefore, for a counterlaid construction, the stiffness in the circumferential (hoop) direction (where wires are in line contact) is much greater than in the radial sense, and it is this key property that is used to set up a series of nonlinear compatibility equations to obtain the normal forces over the various contact patches throughout the structure.

With this information to hand, the compliances for a perturbation of a given type and size can be found, as can interwire movements and changes in wire strain. From the properties of the sheets and wires, simple transformations and summation lead to estimates of axial and torsional stiffnesses whose corresponding hysteresis under uniform cyclic loading can also be estimated (Raoof and Hobbs 1988a, b).

It is recognized that there are uncertainties in calculating the line-contact (i.e., hoop) stresses in a real cable because of the random irregularities of fit of the wires within the strand. The variations are a function of the method of manufacture and life history of the strand. Carefully conducted large-scale experiments (Raoof 1990a) have demonstrated that because of the very gradual nature of interwire/interlayer fretting, cables may need (depending on their construction) a lengthy period of working-in for their internal structure to become reasonably stabilized. In this period cable hysteresis (which is largely controlled by line contact of wires in the same layer) was found to change in a very complex way. In long-term applications, however, fully bedded-in cables assume a reasonably stable internal structure, with the wires in the same layer touching each other (Raoof 1990a). Calculation of pitch circle radii for the individual layers in long-term applications may, therefore, be based on the assumption that wires in line contact are just touching each other. Because of interwire/interlayer abrasion and local contact deformations, measurements of cable outer diameter (Hobbs and Raoof 1982) confirm that the simple adding up of individual wire diameters will not give a reasonable figure for pitch circle radii in the individual layers and (the rather significant) degree of bedding-in at the interlayer trellis points of contact must be taken into account. The orthotropic sheet theory has been developed for large-diameter and multilayererd spiral strands (Raoof and Hobbs 1988b), for which it can be theoretically shown (Raoof and Hobbs 1988a) that estimates of interwire/interlayer contact forces are fairly insensitive to the exact value assumed for the pitch circle radii of the individual layers and a reasonable estimate is all that is required.

Simple charts for obtaining reliable estimates of strand axial stiffness and various kinematic parameters (such as wire strains and movements) have been developed in Raoof and Hobbs (1988a) and the relevant information directly applicable to our present purposes will be briefly summarized.

Theory

In repeated (cyclic) loading regimes, the tangential stiffness has been shown to be related to the magnitude of load perturbation about the mean axial load (Hobbs and Raoof 1982). The stiffness is larger for small load disturbances, which are unable to initiate full interwire slip, than those for large disturbances, which induce full slip between the wires in various layers. A wide range of results for elastic moduli are available for strands as a result of predelivery checks and bedding-in by the manufacturers: these results are invariably "full-slip" moduli in the present terminology because of the large load range involved. Parametric studies have shown (Raoof and Hobbs 1988a) that the full-slip axial stiffness of strands with both ends fixed against rotation can be predicted for any construction as a function of a simple parameter, H, where

$$H = \sum_{i=1}^{N} \frac{A_{Ni}}{A_T} \cos^4\alpha_i \qquad (1)$$

where N = the total number of layers; and α_i = the lay angle in layer i whose net steel area is A_{Ni}, where

$$A_{Ni} = \pi n_i \left(\frac{D_i}{2}\right)^2 \sec\alpha_i \qquad (2)$$

where D_i = wire diameter; and n_i = number of wires, with

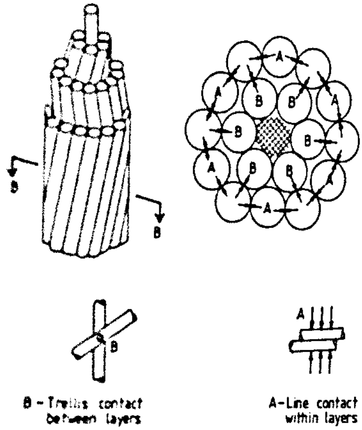

FIG. 1. Pattern of Interwire/Interlayer Contact Forces

$$A_T = \sum_{i=1}^{N} A_{Ni} \qquad (3)$$

The full-slip strand axial stiffness, $E_{\text{full-slip}}$, is then found from

$$\frac{E_{\text{full-slip}}}{E_S} = -0.26442 - 2.0046H + 6.5735H^2 - 3.3068H^3 \qquad (4)$$

where E_s = steel Young's modulus.

The axial strain, S_1, in the individual layers with lay angle α, due to strand axial strain, S_1', is given by

$$\frac{S_1}{S_1'} = 1 - 0.00255\alpha + 0.000215\alpha^2 - 0.0000271\alpha^3 \qquad (5)$$

where α is in degrees.

The change in the lay angle, $d\alpha_i$, in various layers is related to α by

$$\frac{d\alpha}{S_1'} = 0.0203\alpha - 0.000576\alpha^2 + 0.0000395\alpha^3 \qquad (6)$$

where α is in degrees and $d\alpha$ is in radians.

Eqs. 4–6 are third-order polynomials fitted into the results obtained from parametric studies on the orthotropic sheet model. They cover the practical range of $0 < \alpha < 25°$. The interwire rotation over individual trellis points of contact, Fig. 1, between neighboring layers i and $i + 1$ is

$$\omega = d\alpha_i - d\alpha_{i+1} \qquad (7)$$

where $d\alpha$ is positive for right-hand lay.

Full details of a simple method for calculating the magnitude of interwire/interlayer contact forces in various layers of an axially loaded multilayered helical strand are given in Raoof and Hobbs (1988a).

Trellis-Contact Torsional Movements

In their study of the axial fatigue problem, Knapp and Chiu (1988) neglected the relative motions between wire layers. The present orthotropic sheet model gives the magnitude of trellis interlayer movements, which, for sections away from terminations, is in the form of pure rotation over interlayer points of contact. Note that plane sections in the free field (away from end effects) remain plane during cable axial deformation.

In the general field of contact stress theory, torsional contact of nonspherical bodies has been investigated by several authors, including Cattaneo (1955) and Pacelli (1956). The latter author constructed an exact solution for the general case of contact between two nonspherical bodies under an initially applied normal load, on which is superimposed a monotonically increasing torsional loading on the contact patch.

For an elliptical contact patch carrying a constant normal load, P, and a monotonically increasing torque, M, the torque causes the spread of an annular region of slip from the outer edge of the contact towards the center of the patch, until adhesion is completely lost and gross sliding takes place. At the onset of gross sliding the maximum torque, M_{max}, is given by Cattaneo (1955) as

$$M_{max} = \frac{3f'Pa}{32}\left(1 - \frac{\gamma}{\beta}\right) \quad (8)$$

where f' = coefficient of friction; and

$$\gamma = \frac{\eta B_2(a^2 - b^2) + 2\xi(B_1 b^2 - B_2 a^2)}{2\eta[\eta B_1 B_2(a^2 - b^2) + \xi(B_1 + B_2)(B_1 b^2 - B_2 a^2)]} \quad (9a)$$

$$\beta = \frac{-\eta B_1(a^2 - b^2) + 2\xi(B_1 b^2 - B_2 a^2)}{2\eta[\eta B_1 B_2(a^2 - b^2) + \xi(B_1 + B_2)(B_1 b^2 - B_2 a^2)]} \quad (9b)$$

where

$$B_1 = \frac{\pi}{b(a^2 - b^2)}[a^2 E(e) - b^2 K(e)] \quad (9c)$$

$$B_2 = \frac{\pi b}{a^2 - b^2}[K(e) - E(e)] \quad (9d)$$

and

$$\eta = \frac{1}{\pi\mu} \quad (9e)$$

$$\xi = \frac{\lambda}{2\pi\mu(\lambda + \mu)} \quad (9f)$$

λ and μ are Lame's constants of an elastic material, where

$$\lambda = \frac{\nu E_s}{(1 + \nu)(1 - 2\nu)} \quad (9g)$$

$$\mu = \frac{E_s}{2(1 + \nu)} \quad (9h)$$

where a and b = semimajor and semiminor axes of the contact patch (Raoof 1990b); and $K(e)$ and $E(e)$ = complete elliptic integrals of the first and second kind, respectively (Jahnke and Emde 1945) with argument e given by

$$e = \left(1 - \frac{b^2}{a^2}\right)^{1/2} \qquad (10)$$

For the partial slip regime, the semimajor and semiminor axes of the no-slip part of the contact patch, a^* and b^*, are related to the induced angular rotation, ω, by (Pacelli 1956)

$$\omega = -\frac{3f'P}{\pi^2 b\beta}[K(k') - E(k')] \qquad (11a)$$

where

$$k' = \sqrt{1 - \theta^2} \qquad (11b)$$

and

$$\theta = \frac{a^*}{a} = \frac{b^*}{b} \qquad (11c)$$

For the no-slip case (i.e., the initial tangent to M-versus-ω plot), Cattaneo (1955) gives

$$M = \frac{2}{3}\pi ab(\gamma - \beta)\omega \qquad (12)$$

Eqs. 11a–c only give the relationship between the parameter θ and rotation, ω, with the normal force on the contact patch remaining constant. With an axial load perturbation on the strand, the oscillating component of the normal force, P, will have some influence on the magnitude of the resulting ω. The writer has not traced a full analysis of this situation. Moreover, presently available literature in the general field of contact does not offer solutions for cycling loading. Nevertheless, at least for small levels of range to mean ratio of strand axial load, Eqs. 8–12 may be used to give an idea of the extent of the spread of the partial slip annulus (i.e., the $a^*/a = b^*/b$ values) over the trellis contact patches. This, then, gives a reasonable indication of the severity of damage induced in the wires under fretting fatigue conditions due to interwire/interlayer rotation.

For each strand construction, the following steps should be taken.

1. Use Eqs. 1–4 to obtain an estimate of strand axial stiffness.
2. For an assumed level of mean axial load, calculate the strand axial strain, S_1', and hence the corresponding axial wire strains, S_1, in individual layers throughout the cable (Eq. 5).
3. The mean value of the normal force on the individual trellis points of contact between all the layers may be obtained by the method given in Raoof and Hobbs (1988a).
4. Use the method in Raoof (1990b) to find the size (a and b) of the contact patches under the mean trellis normal loads.
5. For each assumed level of cable axial load perturbation superimposed on

TABLE 1. 1 × 92 Wire Strand, 39-mm Outer Diameter, Ultimate Tensile Strength = 1.23 MN

Layer (1)	Number of wires (n) (2)	Lay direction (3)	Wire diameter D (mm) (4)	Lay angle α (degrees) (5)	Pitch circle radius r (mm) (6)
1	30	Right hand	3.54	17.74	17.73
2	24	Left hand	3.54	16.45	14.10
3	18	Left hand	3.54	15.93	10.57
4	12	Right hand	3.54	14.90	7.04
5	7	Right hand	3.54	15.42	4.19
King	1	—	5.05	—	—

the mean, calculate the corresponding cable axial strain perturbation and then use Eqs. 6 and 7 to find the magnitude of the rotation, ω, over the individual trellis points of contact.

6. Use Eqs. 8–10, which give the magnitude of the maximum trellis point torque, M_{max}.

7. Solve Eqs. 11a–c to give estimates of the extent of partial slip regime [i.e., $(a^*/a) = (b^*/b)$ values].

Results for Interlayer Slippage

Table 1 gives construction details for a realistic multilayered 39-mm-diameter strand with a maximum breaking load of 1.23 MN. Fig. 2 shows variations of a^*/a of the individual trellis points of interlayer contact as a function of cable axial load perturbation for two different levels of mean axial load. The 39-mm specimen is of a torque-balanced construction with subtle variations of lay angle and direction in its various layers. Layers 1 and 2 are of opposite lay and hence undergo substantially higher levels of interlayer rotation than, for example, layers 2 and 3, which are of the same lay direction. The assumed value of the coefficient of friction f' is 0.12, which has been found to be a realistic figure in long-term applications (Hobbs and Raoof 1982; Raoof and Hobbs 1988b).

Fig. 2 illustrates that for the practical range of axial load perturbations, the spread of the partial slip zone over the trellis points of contact is not very significant. Indeed, it is demonstrated that gross sliding is unlikely to occur. On the other hand, theoretical results (backed by experimental observations) strongly suggest (Raoof and Hobbs 1982) that gross sliding over the line contacts between various wires in any given layer start at much lower levels of range to mean ratio of axial load. The principal source of strand overall hysteresis is therefore the interwire line-contact slippage. However, experimental observations suggest that wire breakages (away from terminations) are predominantly located over the trellis contact points. This is believed to be a result of high levels of stress concentration at these locations.

Contact Stresses

The principal stresses $\sigma_1(z)$, $\sigma_2(z)$, and $\sigma_3(z)$ directly under the center of the trellis contact patches at a depth z below the surface may be computed

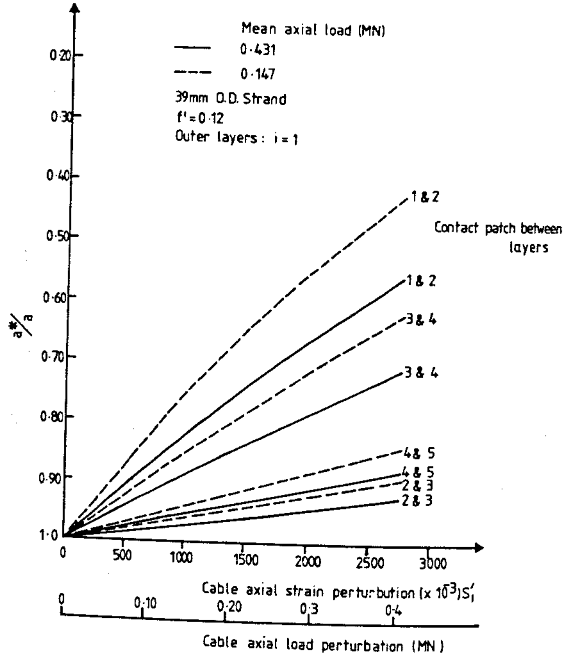

FIG. 2. Contact Patch Partial Slip in Various Layers of 39-mm Specimen

using the closed-form solutions of Thomas and Hoersh (1930) as summarized by Knapp and Chiu (1988).

The Von-Mises effective stress may then be computed from

$$\sigma'(z) = \left\{\frac{[\sigma_1(z) - \sigma_2(z)]^2 + [\sigma_2(z) - \sigma_3(z)]^2 + [\sigma_3(z) - \sigma_1(z)]^2}{2}\right\}^{1/2} \quad \ldots\ldots (13)$$

For a given mean axial load and contact patch, the maximum value of $\sigma'(z)$ occurs at distance $z_{\max}$ from the surface, which may be found numerically by, for example, a three-point search.

Fig. 3 shows the variations of the maximum Von Mises stress with the level of mean axial load (expressed as a percentage of maximum breaking load) for three rather different strand constructions with 16.4, 39, and 51 mm diameter (Tables 1–3). The 16.4-mm strand has only two layers of opposite lay over a king wire, while the 39-mm and 51-mm strands are composed of five layers of wires over the central core, which, in the case of the latter strand, consist of a series of equal lay wires. Apart from the outer and penultimate layers, only layers 3 and 4 of these two strands are of opposite lay with consequent substantial levels of contact stresses.

The significantly high levels of Von Mises stresses will, for the first application of loading, cause plastic flow in the wire material. However, as pointed out by Archard (1957), although it is reasonable to assume plastic flow for the first few loading cycles, it is unrealistic to assume this for surfaces that make millions of contacts, as is the case for long-term fatigue studies. The contact patches may flow plastically at first, but they must reach

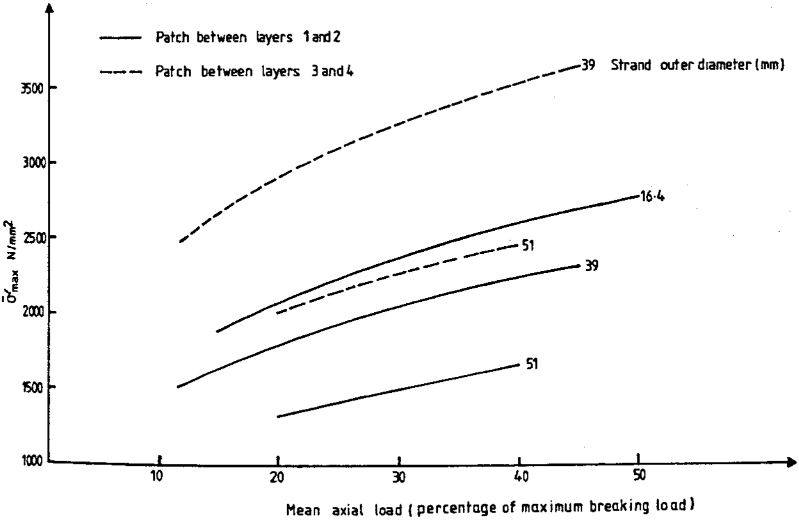

FIG. 3. Pattern of Maximum Von Mises Contact Stress for Various Strand Constructions

TABLE 2. 1 × 19 Wire Strand, 16.4-mm Outer Diameter, Ultimate Tensile Strength = 0.234 MN

Layer (1)	Number of wires (n) (2)	Lay direction (3)	Wire diameter D (mm) (4)	Lay angle α (degrees) (5)	Pitch circle radius r (mm) (6)
1	12	Right hand	3.25	11.91	6.41
2	6	Left hand	3.25	11.42	3.30
King	1	—	3.594	—	—

TABLE 3. 1 × 139 Wire Strand, 51-mm Outer Diameter, Ultimate Tensile Strength = 2.16 MN

Layer (1)	Number of wires (n) (2)	Lay direction (3)	Wire diameter D (mm) (4)	Lay angle α (degrees) (5)	Pitch circle radius r (mm) (6)
1	36	Right hand	4.01	12.83	23.59
2	30	Left hand	4.01	12.63	19.65
3	24	Left hand	4.01	12.35	15.72
4	18	Right hand	4.01	11.94	11.79
5	12	Right hand	4.01	11.14	7.89
Core	6	—	2.31	7.74	—
Core	6	—	3.00	6.71	—
Core	6	—	2.84	4.05	—
Core	1	—	3.00	—	—

a steady state in which the load is supported elastically. The estimates of stress concentration factors based on linear elastic behavior are believed to be on the conservative side.

Stress Concentration Factor

Eq. 5 gives the nominal axial strain in each wire, $\bar{S}_1$, under a mean cable axial strain, $\bar{S}'_1$, which may be used to obtain the nominal wire axial stress $\bar{\sigma}' = E_s\bar{S}_1$. Using Eq. 13 for the effective maximum Von Mises contact stress at depth Z, $\bar{\sigma}'_{\max}$, the stress concentration factor is defined as

$$K_s = \frac{\bar{\sigma}'_{\max}}{\bar{\sigma}'} \quad (14)$$

Since K_s varies with the applied tension, it is assumed that its value at the mean tension can be used for the entire load range.

Fatigue Analysis

Single-Wire Fatigue

Extensive experimental studies of individual wire fatigue have been carried out by many investigators, and the effects of parameters such as carbon content, method of manufacture (e.g., heat treatment and the percentage reduction in wire diameter), surface condition, and surface coatings on wire fatigue life have been widely reported (e.g., Bahke 1980a, b). The available fatigue data generally exhibit a very large degree of scatter even for apparently very similar materials and types of tests (Birkenmaier 1980).

For steel wires the fatigue stress-number of cycles plot (S-N curve) possesses an endurance limit S', below which no damage occurs. Traditionally the magnitude of S' is compared to the ultimate wire stress, S_{ult}: fatigue tests on single galvanized wires suggest (Thorpe et al. 1985) the approximate value of $S' = 0.27\ S_{\text{ult}}$. The reduced magnitude of the endurance limit, S_e, which takes interwire contact and fretting plus surface conditions and size effects, etc., into account may be defined as

$$S_e = K_a K_b S' \quad (15)$$

where K_a = surface finish factor; and $K_b = (1/K_s)$ (Knapp and Chiu 1988). The fatigue life, N_c, of galvanized wires under pure axial tension may then be reasonably defined by

$$N_c = 10^{-(C_2/C_1)} \cdot S_f^{1/C_1} \quad (16a)$$

where

$$C_1 = -\frac{1}{2.24} \log \frac{0.344\ S_{\text{ult}}}{S_e} \quad (16b)$$

$$C_2 = \log 0.344\ S_{\text{ult}} + 2.13 \log \frac{0.344\ S_{\text{ult}}}{S_e} \quad (16c)$$

Eqs. 16*a–c* represent the S-N curve for hot-dipped galvanized wires with $S_{\text{ult}} = 1{,}840\ \text{N/mm}^2$ (Thorpe et al. 1985). Using a Goodman diagram (Shigley 1977), the equivalent fatigue stress, S_f, for finite fatigue life may be found from

$$\frac{\sigma'_a}{S_f} + \frac{\sigma'_m}{S_{ult}} = 1 \quad \text{(17)}$$

where σ'_a and σ'_m = the alternating and mean components, respectively, of the nominal wire axial stresses whose value is given by

$$\sigma'_a = \frac{\sigma'_{max} - \sigma'_{min}}{2} \quad \text{(18a)}$$

$$\sigma'_m = \frac{\sigma'_{max} + \sigma'_{min}}{2} \quad \text{(18b)}$$

where σ'_{max} and σ'_{min} = the nominal wire axial stresses occurring at the maximum and minimum values of superimposed cyclic cable axial load, T_{max} and T_{min}. Eqs. 16*a–c* are valid for fatigue lives of up to $N_C = 10^7$ cycles (endurance limit). For $N_c > 10^7$, the S-N curve possesses a knee whose corresponding endurance stress is S_e.

Fatigue Analysis: Results

Fig. 4 compares the theoretical predictions with experimental fatigue results on the 51-mm-diameter specimen (with construction details given in Table 3). The criterion for fatigue initiation has been the occurrence of first wire failure in the outer layer. With epoxy resin end terminations, all the

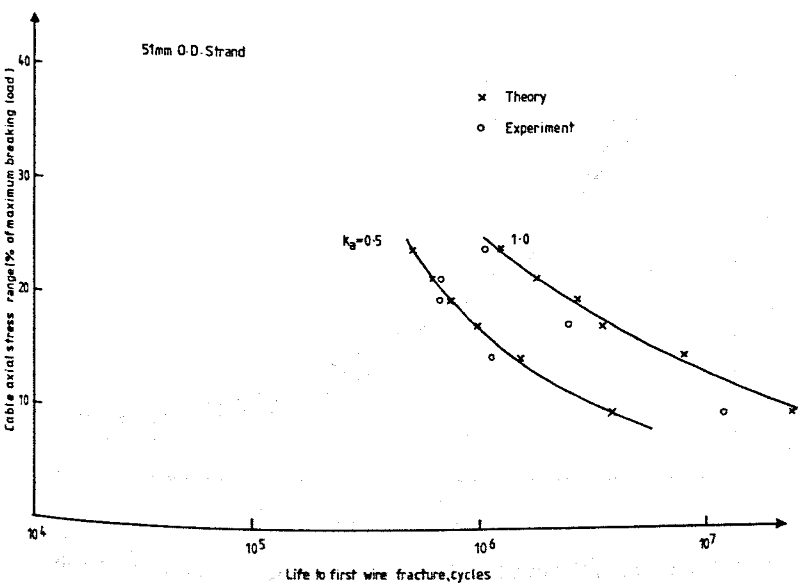

FIG. 4. Comparison of Theory and Experimental Fatigue Data for 51-mm Strand

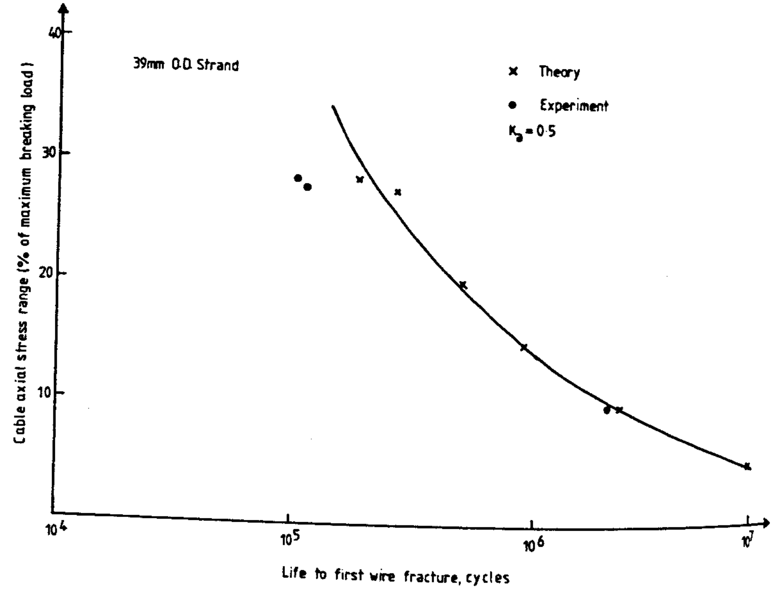

FIG. 5. Comparison of Theory and Experimental Fatigue Data for 39-mm Strand

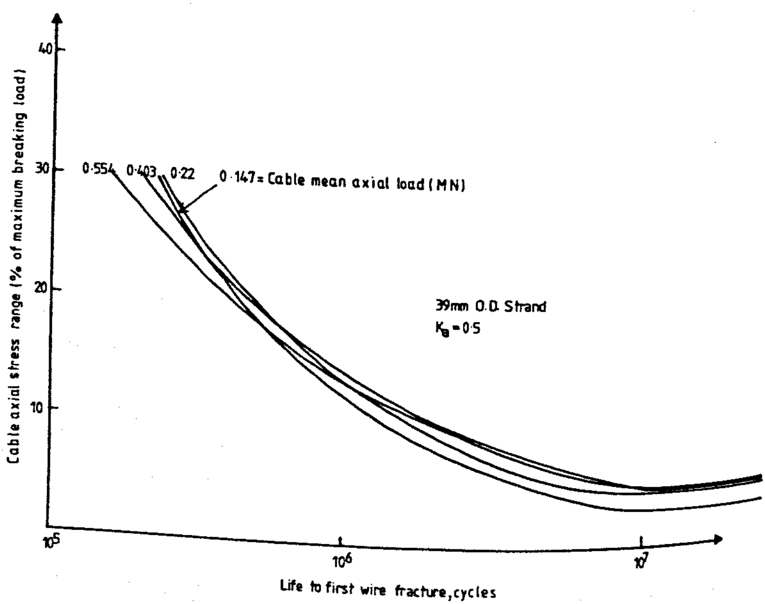

FIG. 6. Effect of Various Levels of Mean Axial Load on Strand Fatigue Life

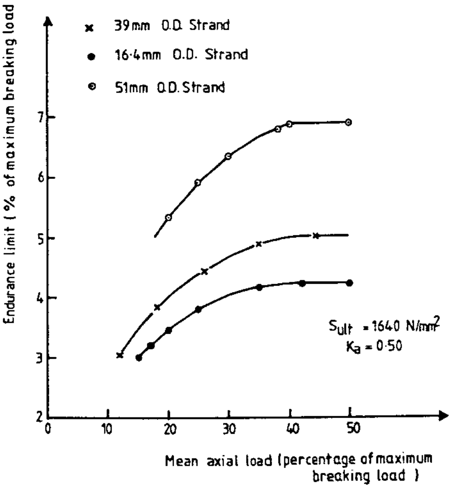

FIG. 7. Comparison of Endurance Limit for Various Strand Constructions and Levels of Mean Axial Load

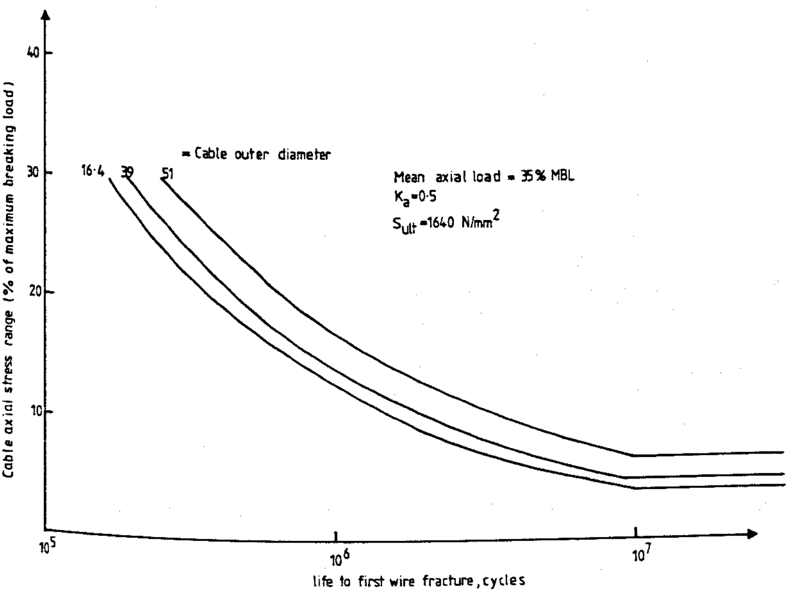

FIG. 8. Comparison of Fatigue Life to First Outer Layer Wire Fracture for Various Strand Constructions

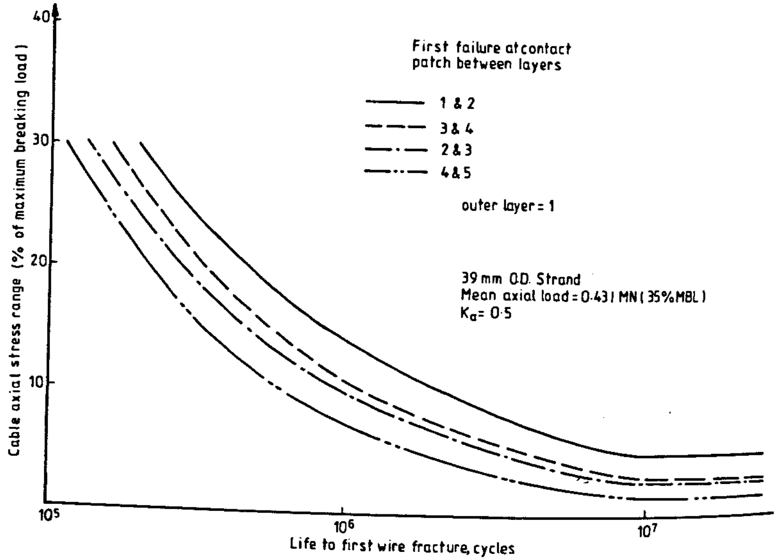

FIG. 9. Comparison of Fatigue Life of First Inner and Outer Wire Fractures for 39-mm Strand

wire failures occurred away from the ends (in the free field). A fairly significant degree of scatter was found in the experimental data, which may be covered by the empirical surface finish factor K_a in the range $0.5 \leq K_a \leq 1.0$. The ultimate tensile strength of the wire material is $S_{ult} = 1{,}640\ \mathrm{N/mm^2}$. Fig. 5 compares the fatigue life to the first outer wire fracture with theory for the 39-mm specimen whose end terminations were zinc-poured sockets (Hobbs and Ghavami 1982). The reported wire fractures on the long (6-m) specimens were invariably located at the mouth of the socket, which acted as a stress raiser. Even with $K_a = 0.5$, the theory gives an upper-bound solution (as expected). Fig. 6 shows the effect of the level of mean axial load on the cable S-N curve. Even for a given level of mean axial load, reported cable experimental fatigue data often exhibit a significant degree of scatter, which may easily mask these secondary variations in cable S-N curves under various levels of mean axial load.

From Fig. 7, the endurance limit (for a given wire material) depends on the type of construction, and, for a given cable, increases with increasing level of mean axial tension approaching a constant value at around 40% of maximum cable-breaking load. This is of particular importance in offshore applications, where the small-amplitude forces are the ones with the highest number of occurrences. Therefore, it is concluded that small-amplitude/long-life testing is necessary for these applications.

The effect of strand construction on fatigue life to first outer-layer wire fracture in the free field is shown in Fig. 8, which assumes the same type of wire material for all three constructions. Fig. 9 shows the theoretical prediction that the first wire failure is likely to occur inside the 39-mm strand. Widely used fatigue damage criteria based on the number of visual (outer-layer) wire failures may thus be unconservative and particular attention must be paid to alternative methods of nondestructive inspection capable of detecting inner wire failures.

Summary and Conclusions

Previously reported orthotropic sheet theory has been used to obtain estimates of interwire contact stresses in realistic pretensioned multilayered structural strands. Using these data with axial fatigue data on single wires, estimates of strand fatigue life to first wire fracture under uniform cyclic axial loading have been obtained. The theory also casts some light on the relevance of cross-wire (trellis) interlayer movements (and hence fretting) to strand axial fatigue (and hysteretic) performance. The theoretical predictions for some large-diameter strands have been reasonably supported by experimental fatigue data. The theory throws some light on the influence of the level of mean axial load and type of strand construction on strand fatigue performance in long-term applications. For a given wire material, endurance limit is found to increase with increasing levels of mean axial load, becoming practically constant for mean axial loads greater than 40% of cable maximum breaking load. Various cable constructions are also likely to exhibit significantly different levels of endurance limit.

Acknowledgments

The writer acknowledges the long-standing and friendly cooperation of British Ropes' Personnel at Doncaster. In particular, he is grateful for their permission to publish their fatigue experimental results of Fig. 4, on the 51-mm-diameter specimen.

Appendix I. References

Archard, J. F. (1957). "Elastic deformation and the laws of friction." *Proc. Royal Soc. London*, London, U.K., A243, 190–205.
Bert, C. W., and Stein, R. A. (1962). "Stress analysis of wire rope in tension and torsion." *Wire and Wire Products*, 37, 769–770, 772, 816.
Bahke, E. (1980a). "Principles defining the strength of wire ropes and chains. I." *Wire*, 29(2), 54–61.
Bahke, E. (1980b). "Principles defining the strength of wire ropes and chains." *Wire*, 30(3), 168–176.
Birkenmaier, M. (1980). "Fatigue resistant tendons for cable-stayed construction." *IABSE Proc.*, International Association for Bridge and Structural Engineering, 30/80, 65–69.
Cattaneo, C. (1955). "Compressione e torsione nel Contatto tra corpi elastici di forma qualunque." *Ann. Scuola Norm. Sup. pisa*, Ser III (9), 23–42 (in Italian).
Chaplin, C. R., and Potts, A. E. (1988). "Wire rope in offshore applications." *Publication 88/100*, Marine Tech. Directorate Ltd., London, U.K.
Chien, C. H., LeClair, A., Costello, G. A. (1988). "Strength and fatigue life of wire rope." *Mech. of Structs. and Machines*, 16(2), 213–223.
Hobbs, R. E., and Raoof, M. (1982). "Interwire slippage and fatigue prediction in stranded cables for TLP tethers." *Behavior of Offshore Structures, Proc. 3rd Int. Conf. Behavior of Offshore Structs.*, C. Chryssostomidis and J. J. Connor, eds., Hemisphere Publishing/McGraw-Hill, New York, N.Y., 77–99.
Hobbs, R. E., and Ghavami, K. (1982). "The fatigue of structural wire strands." *Int. J. Fatigue*, 4, 69–72.

Jahnke, E., and Emde, F. (1945). *Tables of functions*. Dover Publications, New York, N.Y.

Knapp, R. H., and Chiu, E. Y. C. (1988). "Tension fatigue for helically armored cables." *J. Energy Resour. Tech.*,1 10(Mar.), 12–18.

Leissa, A. W. (1959). "Contact stresses in wire ropes." *Wire and Wire Products*, 34(3), 372–373.

Pacelli, M. (1956). "Contatto con attrito tra due corpi elastici di forma qualunque: compressione e torsione." *Ann. Scoula Norm. sup. pisa*, III(10), 155–184 (in Italian).

Phillips, J. W., Miller, R. E., and Costello, G. A. (1980). "Contact stresses in a straight cross-lay wire rope." *1st Annual Wire Rope Conf.*, Denver, Colo., Mar., 177–200.

Raoof, M. (1990a). "Comparison between the performance of newly manufactured and well-used spiral strands." *Proc.*, Institution of Civil Engineers, II, 89(1), 103-120.

Raoof, M. (1990b). "Free bending of spiral strands." *J. Engrg. Mech.*, ASCE, 116(3), 512–530.

Raoof, M., and Hobbs, R. E. (1988a). "Analysis of multilayered structural strands." *J. Engrg. Mech.*, ASCE, 114(7), 1166–1182.

Raoof, M., and Hobbs, R. E. (1988b). "Torsion tests on large spiral strands." *J. Strain Analysis Inst. Mech. Engrs.*, London, U.K., 23(2), 97–104.

Shigley, J. E. (1977). *Mechanical engineering design*. McGraw-Hill, New York, N.Y.

Starkey, W. L., and Cress, H. A. (1959). "An analysis of critical stresses and modes of failure of a wire rope." *J. Engrg. for Industry*, 81(B4), 307–316.

Thomas, H. R., and Hoersh, V. A. (1930). "Stresses due to the pressure of one elastic solid upon another." *Bulletin No. 212*, Engrg. Exp. Sta., Univ. of Illinois, 26(46), Urbana, Ill.

Thorpe, T. W., Rance, A., and Silvester, D. R. V. (1985). "The fatigue of electrogalvanised wire used in the manufacture of wire ropes." *Report by Materials Development Div.*, Atomic Energy Research Establishment (AERE), Harwell, U.K., Jan.

APPENDIX II. NOTATION

The following symbols are used in this paper:

A_{Ni} = net steel area in layer i;

A_T = $\Sigma_{i=1}^{N} A_{Ni}$;

a, b = semimajor, semiminor axes;

a^*, b^* = semimajor, semiminor axes of no-slip part of contact patch;

B_1, B_2 = constants in Cattaneo's problem;

D = wire diameter;

$E_{\text{full-slip}}$ = full-slip axial cable modulus;

E_s = Young's modulus for steel;

e = $[1 - (b^2/a^2)]^{1/2}$;

f' = coefficient of friction;

K_a = surface finish factor;

K_b = $1/K_s$;

$K(e), E(e), K(k'), E(k')$ = complete elliptic integrals of first and second kind;

K_s = stress concentration factor;

k = (b/a);

k' = modulus of elliptical integral = $\sqrt{1 - [(a^*/a)]}$;

M = torque on contact patch;
M_{max} = maximum torque on contact patch;
N = number of layers;
N_C = number of cycles to fatigue failure;
n_i = number of wires in layer i;
P = normal load on trellis contact patch;
S_1 = wire axial strain;
S_1' = cable axial strain;
S' = endurance stress for bare wire;
S_e = wire endurance stress under interwire contact;
S_f = equivalent fatigue stress range;
S_{ult} = wire ultimate strength;
T_{max}, T_{min} = maximum and minimum cable tension;
α_i = lay angle in layer i;
$d\alpha$ = change in lay angle (radians);
γ, β = constants in Cattaneo's problem;
ν = Poisson's ratio;
$\sigma_1, \sigma_2, \sigma_3$ = principal stresses;
$\bar{\sigma}'$ = mean wire nominal axial stress;
σ_a' = wire nominal stress range;
σ_m' = mean wire nominal stress;
$\sigma'(z)$ = Von Mises contact stress;
$\bar{\sigma}'_{max}$ = maximum Von Mises contact stress;
$\sigma'_{max}, \sigma'_{min}$ = maximum and minimum nominal wire stresses; and
ω = trellis contact angular rotation.